Results in Engineering 26 (2025) 105459

Contents lists available at ScienceDirect

Results in Engineering

journal homepage: www.sciencedirect.com/journal/results-in-engineering

Research paper

Design and studies of monopole antenna integrated with metamaterial-based CSRR and rectangular spiral shaped for super wide band application ☆

Nurhayati Nurhayati [a,*], Fitri Yuli Zulkifli [b], Ali Hanafiah Rombe [c], Rohim Aminullah Firdaus [d], Muhammad Fauzan Edy Purnomo [e], Minh Thuy Le [f], Ahmed J.A. Al-Gburi [g,*]

[a] Department of Electrical Engineering, Universitas Negeri Surabaya, Surabaya, 60231, Indonesia
[b] Department of Electrical Engineering, Universitas Indonesia, 16435, Depok, Indonesia
[c] Department of Electrical Engineering, Universitas Sumatera Utara, Medan, Indonesia
[d] Department of Physics, Universitas Negeri Surabaya, Surabaya, 60231, Indonesia
[e] Department of Electrical Engineering, Universitas Brawijaya, Malang, Indonesia
[f] School of Electrical and Electronic Engineering, Hanoi University of Science and Technology, Hanoi, Viet Nam
[g] Center for Telecommunication Research & Innovation (CeTRI), Fakulti Teknologi Dan Kejuruteraan Elektronik Dan Komputer (FTKEK), Universiti Teknikal Malaysia Melaka (UTeM), Jalan Hang Tuah Jaya, Durian Tunggal, Melaka, 76100, Malaysia

ARTICLE INFO

Keywords:
CSRR
Monopole antenna
Metamaterial
Notch-band frequency
Super wideband antenna

ABSTRACT

Telecommunications technology in the Super Wide Band (SWB) frequency is crucial for numerous applications including short- and long-distance communication. This study examines the effect of wavy structure at the top edge of the patch, the variation of ground height, the shape and the location of Complimentary Split Ring Resonator (CSRR), and square spiral structure to a semi-elliptical monopole antenna performance. Parametric studies were used to evaluate the antenna's reflection coefficient, directivity, band notched frequency, and axial ratio. Simulation results show that the antenna has a reflection coefficient of less than -15 dB at most frequencies from 0.38 to more than 20 GHz. The Wavy structure type A monopole antenna has a directivity of 6.12 dBi at 2 GHz, whereas type B has 3,985 dBi. However the highest gain for Antenna Type-C is 7.45dBi. Especially at low frequencies, ground height affects antenna return loss. Several notched band frequencies and circular polarization can be generated on the antenna by providing a rectangular spiral structure on the groundplane or a CSRR structure at the base of the patch. The minimum axial ratio (AR) is 1.11 dB at frequencies from 5.965 GHz to 6.585 GHz and 0.56 dB at 2 GHz when the spiral structure height is varied. There is agreement on the antenna's performance between the experimental and simulation results. The antenna has been utilized in through-wall radar, therefore it can be used to improve Super Wide Band radar and communications systems.

1. Introduction

Planar antennas which can work in wide bandwidth frequencies are of interest in the civil [1][2], industrial [3], military sectors [4], radar [5], vehicle mobilization systems [6], product identification [7], wearable device [8], microwave imaging [9], 5G [10] and so on. UHF-frequency antennas have increasingly proliferated during the previous decade. They are also utilized for RFID communications, tracking, Automatic Toll Collection, the aviation industry, the Internet of Things, human identification, retail management, transportation logistics, and other applications [11]. Recently, a combination of ultra-wideband (UWB) and narrowband ultrahigh frequency (UHF) technologies was

☆ This work was supported in part by the Indonesia Collaboration Research Funding from Legal-Entity State Higher Education Institutions (Universitas Negeri Surabaya, Universitas Indonesia, and Universitas Sumatera Utara); in part by Riset Kolaborasi Indonesia (RKI), Universitas Negeri Surabaya (Indonesia), under Grant B/43856/UN38.III.1/LK.04.00/2024.

* Corresponding authors.
E-mail addresses: nurhayati@unesa.ac.id (N. Nurhayati), yuli@eng.ui.ac.id (F.Y. Zulkifli), ali3@usu.ac.id (A.H. Rombe), rohimfirdaus@unesa.ac.id (R.A. Firdaus), mfauzanep@ub.ac.id (M.F.E. Purnomo), thuy.leminh@hust.edu.vn (M.T. Le), ahmedjamal@utem.edu.my (A.J.A. Al-Gburi).

https://doi.org/10.1016/j.rineng.2025.105459
Received 28 January 2025; Received in revised form 1 May 2025; Accepted 22 May 2025
Available online 27 May 2025

presented as a possible choice for 5G's simultaneous wireless power and information transfer, as well as identification and accurate indoor positioning systems for the internet of things. The government and industry have given UHF RFID a lot of attention because of its many interesting benefits, which include high reading rates, long writing distances, multi-target recognition, and fast-moving target identification. This technique is also developing extremely quickly. RFID is a tracking and object identifying system that sends data via radio waves. RFID tags, which are electronic labels affixed to items, provide information to special readers. A transponder, a reader, and a computer for data processing are the three main parts of an RFID system. An antenna built into the reader (interrogator) connects to the TAG [12]. Therefore, the antenna should be inexpensive, light, simple, and easy to fabricate to guarantee efficient communication [13].

In the military field, RFID technology can also be used to support the need for identification of military personnel, medical, volunteers, civilians, etc. With the help of RFID-based IoT models tracking and monitoring of people's movements can also be carried out where data can be collected in real-time. Each nation uses a different UHF RFID operating frequency, which ranges from 902 to 928 MHz in North America, 908.5 to 914 MHz in Korea, 920 to 926 MHz in Australia, 922 to 928 MHz in Taiwan, and 950 to 956 MHz in Japan [14]. Meanwhile, the standard working frequency for RFID readers in Indonesia, issued by the Director General of Posts and Telecommunications, Department of Communications and Information Technology, is 923-925 MHz (UHF). In the UHF band, electromagnetic (EM) wave signals show strong penetrating power and require lower transmit power, hence the UHF band is very suitable for communication in the complex urban areas, as well as other applications such as walkie-talkie communication in dense forests [15]. As a result, the tag antenna is a crucial component of the RFID system. For such, the antenna's excellent performance is required. However, as of now, there has been limited study conducted on the construction of the RFID, UHF, Radar antenna that work at sub 1 GHz wideband frequency.

Notably, there is an increased need for wideband antennas with vertical polarization in the ultrahigh-frequency (UHF) and very high-frequency (VHF) bands. Historically, $\lambda/4$ monopole components might be quite tall at low frequencies. A typical 40 MHz $\lambda/7.5$ monopole is 1.875 m tall above its ground plane and exhibits narrowband characteristics [16]. Antenna research for RFID applications at UHF frequencies has been carried in [17] by adding L shaped in the single layer antenna with a size of 120 mm × 120 mm with an impedance bandwidth of 840-960 MHz. A coin shape antenna with a size of 250 mm × 250 mm with an impedance bandwidth of 22.4% (768-962 MHz) has been discussed in [18]. Research on antennas that operate at UHF frequencies can also be used for radar applications. For example, research [19] that employs a Vivaldi antenna measuring 450 mm × 600 mm can work at frequencies ranging from 470 MHz to 2.8 GHz. Antennas for radar applications aboard ships that can operate at frequencies between 170 and 247.6 MHz have been considered in [20]. These antennas have dimensions of 500 mm × 400 mm using a semi-elliptical dipole antenna. Studies have been conducted on wearable Vivaldi antennas that operate within the frequency range of 3.66–20.42 GHz [8]. This antenna operates at frequencies above 3 GHz, whilst antennas functioning below 1 GHz might be utilized for many applications. The Vivaldi antenna with a dimension of 240 mm × 240 mm has also been investigated for Radar applications and can work in 0.7-2.1 GHz, 1.0-2.1 GHz [21]. Those antennas that operate in the sub-1 GHz region are able to improve their ability to manage interference and reach greater distances. Additionally, there are still a great number of applications that are required in order to connect low-power Internet of Things purposes. However, several antennas that have been created for usage in frequencies lower than one gigahertz have dimensions that are relatively large and do not yet have an extensive bandwidth.

UWB antennas have promising applications [22]in indoor or outdoor communications. There are several obstacles associated with using UWB or SWB frequency. While both "super wideband" (SWB) and "ultra wideband" (UWB) antennas refer to antennas with a very broad operating frequency range, a key difference is that "super wideband" antennas generally cover a significantly wider bandwidth than "ultra wideband" antennas, meaning they can operate across a much larger spectrum of frequencies; essentially, SWB represents an even wider bandwidth compared to the already wide range of UWB antennas. The antenna is classified as UWB with an RBW of 3.42:1, but the SWB antenna possesses a Bandwidth Ratio above 10:1 [23]. Despite benefits of ultra-wide wideband frequency as unlicensed bandwidth such as high data rate, compact system, and so on, one of the major challenges is avoiding interference caused by coexisting narrow microwave frequency bands, namely the IEEE 802.16 WiMAX band (3.3-3.6 GHz), IEEE 802.11a WLAN bands (5.15-5.35, 5.725-5.825 GHz), and ITU 8-GHz band (8.025-8.4 GHz). Antenna research using notched frequency bands has been carried out using EBG structures [24], U-shaped slots [25][26], Pi-shapes with pin dioda [27], S-shaped strip [28], asymmetric/symetry slot and triangle truncated [29]. However, the notched band technique provided uses a more complex additional structure and some use additional electronic circuits which usually only produce one or two notched band frequency bands which also require additional external components. To address these issues, metamaterial structures, such as CSRR, can be utilized to filter undesired frequencies while also enhancing bandwidth performance, miniaturization, mutual coupling reduction, and reduced side lobe levels. In this study, we apply CSRR structures to filter out some undesirable frequencies without using any external components. As a result, a SWB antenna with multiresonance band rejection capabilities is needed.

The antenna, being a front-end telecommunication system that responsible for data transfer or reception. In order to fulfill the requirements of particular applications, circular polarization of antennas is frequently necessary. Circularly polarized antennas have the ability to reduce the effects of multipath fading and enhance the quality of signal transmission. Circular polarization antenna research has been conducted in [30] by using SIW, in [31] by the utilization of meta-surface, in [32] by 2D FSS, in [33] by electronical swichable. However, the utilization of supplementary structures is more challenging and necessitates the integration of external components. In this investigation, the antenna will be rendered more adaptable by constructing a slot structure that can generate circular polarization and function as a notched frequency band. According to various applications, the antenna must have adequate wide bands, flawless performance, compact size, lost cost and also have circular polarization.

According to the findings of this study, we developed a monopole antenna that is capable of operating at extremely broad frequencies. We have obtained research contributions as enumerated below

- We obtain a design for a monopole antenna that is capable of operating at frequencies ranging from 0.38 to more than 20 GHz and has an S_{11} value of less than -15 dB at almost all its working frequencies. The dimensions of the antenna are $0.3\lambda \times 0.25\lambda$, and it is constructed out of FR4 substrate and copper patch. Some antennas that operate at sub 1 GHz (below 1 GHz) frequencies have larger antenna sizes and have small bandwidths.
- We create wavy structure variations of the monopole antenna on the top edge of the patch and variations in ground antenna height to see the performance of the reflection coefficient and directivity of the antenna. From the simulation results, it was found that there was a significant increase in gain and variation of S_{11} by providing a certain wave structure and ground height.
- By including a CSRR (Complimentary Split Ring Resonator) structure into the antenna patch, we are able to achieve performance throughout many resonance notched frequency bands.
- Incorporate a rectangular spiral configuration by adjusting the dimensions and positioning of the spiral to observe the impact on notched frequency bands and circular polarization efficacy.

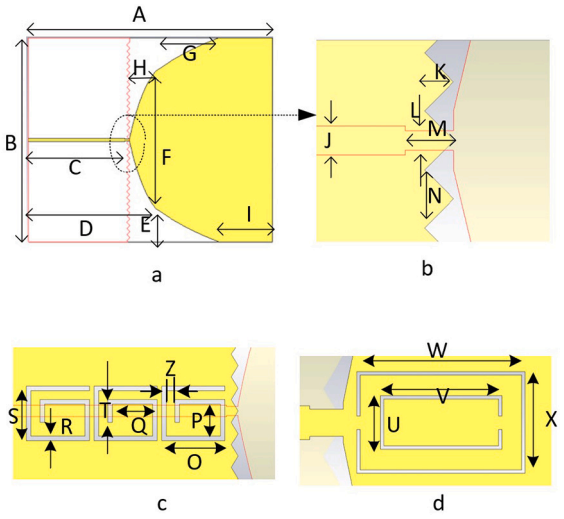

Fig. 1. Geometry of Monopole antena (s) Top View, (b) Back View, (c) Spiral Structure and (d) CSRR Structure.

Table 1
Parameter and antenna dimension in mm.

Par	Dim (mm)	Par	Dim (mm)	Par	Dim (mm)	Par	Dim (mm)
A	240	H	25	O	28	V	18
B	200	I	53	P	14	W	25
C	95	J	3	Q	18	X	15
D	125	K	3	R	2	Y	2
E	32.5	L	2	S	24		
F	135	M	5	T	8		
G	62	N	6	U	8		

- We constructed the antenna and evaluated the S_{11} performance by comparing simulation and measurement results, subsequently applying it to through-wall radar application.

The following sections are presented in such an order: Section 2 details the antenna design. Section 3 analyzes the parametric Study and a conclusion is drawn in Section 4.

2. Antenna design

Fig. 1 shows a monopole antenna consisting of (a) top view monopole antenna, (b) rear view monopole antenna, (c) spiral structure and (d) Rectangular CSRR. The antenna dimensions can be seen in Table 1. The antenna consists of a patch and ground made of copper with a thickness of 0.035 mm and has a substrate made of FR4 material with a permittivity value of 4.3 and the substrat thickness (h) is 1.6 mm. A monopole antenna is built upon a patch antenna that adheres to the following equations (1) to (4) [34]

$$B = \frac{c}{2f\sqrt{\epsilon_{er}}} \tag{1}$$

$$\epsilon_{eff} = \frac{(\epsilon_{er}+1)}{2} + \frac{(\epsilon_{er}-1)}{2}[1+10\frac{h}{B}]\frac{1}{2} \tag{2}$$

$$\frac{\Delta A}{H} = 0.412\frac{(\epsilon_{eff}+0.3)(\frac{B}{h}+0.262)}{(\epsilon_{eff}-0.258)(\frac{B}{h}+0.813)} \tag{3}$$

$$A = \frac{c}{2f\sqrt{\epsilon_{er}}} - 2\Delta A \tag{4}$$

Where B is the dimension of patch Width, A is the patch Length and h is the substrate thickness

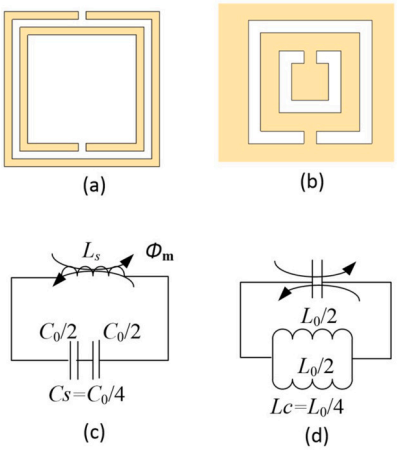

Fig. 2. Rectangular metamaterials: (a) Split Ring Resonator (SRR), (b) Complementary Split Ring Resonator (CSRR), (c) SRR Equivalent Circuit, (d) CSRR Equivalent Circuit.

The antenna supply uses a microstrip line with a neck-like end section so it can increase bandwidth. The ground part is made in a triangular shape where the middle sharp side is right in the middle of the feeding antenna. The curvature of the monopole antenna is determined using the equation (5)

$$y = C_1.e^{Rx} + C_2, C_1 = \frac{y_2 - y_1}{e^{Rx_2} - e^{Rx_1}}, C_2 = \frac{y_1 e^{Rx_2} - y_2 e^{Rx_1}}{e^{Rx_2} - e^{Rx_1}} \tag{5}$$

Where C_1 and C_2 are constants which can be found by entering the values X_1 and X_2. The coordinates X_1, Y_1, are the initial coordinates of the curvature of the curve and X_2, Y_2 are the final coordinates of the curvature of the curve.

Fig. 2 shows the Split Ring Resonator (SRR) and Complimentary Split Ring Resonator (CSRR) and its equivalent circuit. The presence of a CSRR structure can influence antenna resonance and can follow the equation(6) (7):

$$L = \frac{\lambda}{2} = \frac{c}{f_n\sqrt{\epsilon_{eff}}}, n = 1,2,3,4,... \tag{6}$$

$$\epsilon_{eff} = \frac{\epsilon_{er}+1}{2}, \quad f_0 = \frac{1}{2\phi\sqrt{L_s C_s}} \tag{7}$$

where ϵ_{eff} is the equivalent permittivity, c is the speed of light, and where is the CSRR's total length. The notched band can be obtained by adjusting the CSRR's resonance frequency, fn as shown in equation (6) and (7) [23]. Enough proximity between the perimeters of the two split rings is necessary to enhance the stopband suppression effect. By replacing the shunt inductance and shunt inductors with series capacitance, the CSRR can be described as an LC resonator according to the duality principle, as shown in Fig. 2.

$$L_{total} = \frac{4ON - [2N(1+N)] - 3(Z+R)}{N} \tag{8}$$

$$L_{total} = \frac{c}{4fc\sqrt{\epsilon_{reff}}} \tag{9}$$

We also perform complementary Rectangular-shaped spiral structure on the ground and placed in the middle in contact with the feeding line (as shown in Fig. 1). The spiral structure is made in the ground plane and adjacent to different sides of the feeding line so that it can resonate so that the reflection coefficient of the antenna. The dimensions of the spiral can follow the equations (9) (10) referred to in the paper [35]. The performance of an antenna varies based on the length of the inductive arm and the capacitive gap between the arms. For proper resonance, it is necessary that the effective length of the spiral be close to the wavelength corresponding to the resonant frequency.

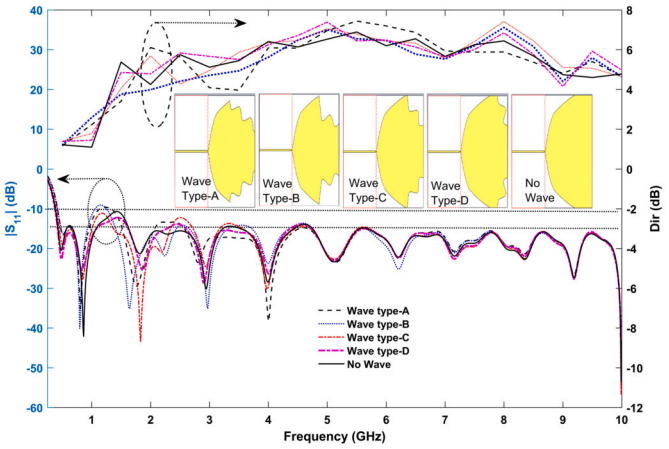

Fig. 3. Coefficient Reflection Magnitude and Directivity performance (at $\theta = 90^0$) of Monopole Antenna with wave variation at the patch.

Fig. 3 explores the monopole antenna by adding the wavy structure type A-D on the edges of both sides of the antenna. The geometry of wave structure follows the equation (10) with the value $A_w = 4$, $B_w = 1$, $C_w = 1$, $D_w = 0.5$ and $L_w = 10$. By changing the wave position, the length, depth, and number of waves will change the geometry and antenna performance.

$$y(t) = A_w(B_w + C_w cos(\frac{D_w \pi t}{L_w})) \quad (10)$$

3. Parametric study

We performed parametric analysis using CST software to determine the impact of antenna geometry on antenna performance in the form of reflection coefficient, gain, surface current, radiation pattern and circular polarization.

3.1. The effect of wavy structure on antenna performance

We conducted a parametric analysis to determine the impact of antenna geometry on antenna performance. Fig. 3 shows five variations in the performance of the reflection coefficient and directivity at theta 90^0 by providing a wavy structure at the edges of both ends of the patch. In this variation, a wavy structure is created following equation (a) by varying the slope and height of the wavy structure. From the simulation results, it is found that variations in waves at the top of the patch do not really affect the performance of the reflection coefficient. This can be seen in Fig. 3 that almost all modifications to the patch still show S_{11} values below -10 dB. In this case we simulate an antenna from 0.25 to 10 GHz and the antenna has an S_{11} of less than -10 dB from 0.37 GHz to more than 10 GHz and almost all specified frequencies have S_{11} < -15 dB except at frequency around frequencies 0.93 GHz to 1.39 GHz. We simulate only up to 10 GHz to save computing time. From the simulation results, S_{11} is found at -10 dB for the low-end frequency at 0.37 GHz for Monopole antenna with Wave type D, while for Wave type B it is at 0.42 GHz. Antennas without wave structures have a minimum S_{11} value of -42.1 dB at a frequency of 0.86 GHz. Meanwhile, Wave type C has a minimum S_{11} at the 1.83 GHz frequency of -43.4 dB. At the 2 GHz frequency, Wave type-A has a directivity of 6.1088 dBi while Wave type-B has a directivity of 3.985 dBi, resulting in an increase in directivity of 2.12 dBi. At a frequency of 3.5 GHz, Wave type C has a directivity of 5,864 dBi while Wave type-A is 3,963 dBi so there is a performance increase of 1.9 dBi. At a frequency of 8 GHz the Wave type-C antenna has a directivity of 7.42 dBi and the Wave type A has a directivity of 5.88 dBi so it has a performance increase of 1.54 dBi. The antenna directivity can be enhanced at certain frequencies while maintaining the antenna bandwidth performance by adjusting the wavy structure on the top and perimeter of the patch. Consequently, this method can be further developed to achieve a higher directivity gain.

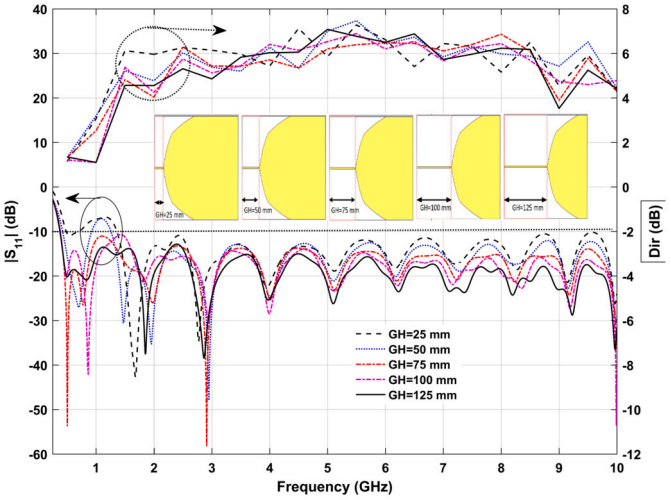

Fig. 4. Reflection coefficient and directivity performance (at $\theta = 90^0$) of Monopole antenna with ground height variation.

3.2. The effect of ground and feeding height on antenna performance

Fig. 4 illustrates the simulation results depicting the performance variation of S_{11} as a function of frequency for a monopole antenna, including alterations in the height of the ground plane and feedline. In this simulation we simulate ground heights of 25 mm, 50 mm, 75 mm, 100 mm and 125 mm using the same substrate size. In this case we setting the lower the ground means the microstrip feeding is also shorter and the patch size is larger. The shorter the microstrip feeding line, the less good the S_{11}'s performance at low end frequencies. From the simulation results it was found that the best performance of the S_{11} was seen at the 0.5 GHz of -53.67 dB for GH 75 mm. At 0.86 GHz, S_{11} was -42.1 dB for GH 100 mm, at the frequency of 1.68 GHz, S_{11} was -42.75 dB for GH 25 and at frequency 2.91 GHz, S_{11} -58.15 dB for GH = 75 GHz. Fig. 4 shows that for Ground Height (GH) 25 mm the S_{11} value is above -10 dB, this is also the case for GH 50 mm. However, at low frequencies, a monopole antenna with GH = 25 mm has the greatest directivity compared to other antennas because the antenna has a larger patch size. At the 1.5 GHz frequency, the order of best directivity performance is for monpoles with GH 25 mm, 100 mm, GH 50 mm, GH 75 mm, and GH 125 mm, namely 6,123 dBi, 5,379 dBi, 5,225 dBi, 4,818 dBi and 4,567 dBi. Variations in ground height will affect return loss performance and directivity performance. At frequencies of more than 4 GHz, the reflection coefficient performance from the best to the worst is obtained by monopole antennas that have GH 125 mm, GH 100 mm, GH 75 mm, GH 50 mm and GH 25 mm. The height of the ground plane and feed line must be taken into account when constructing a monopole antenna since it has a significant impact on the antenna's directivity and S_{11} performance.

3.3. The influence of the CSRR configuration on notched band frequency

Fig. 5 demonstrates the impact of dx (the distance between the CSRR and the antenna's base) on the performance of the reflection coefficient. As can be observed in the section with the circle, the reflection coefficient performance decreases with increasing distance from the CSRR structure to the patch antenna base. The first notched band occurs at frequencies 0.88 GHz to 1.02 GHz with max is -4.16 dB, the second notched band at 1.08-1.29 GHz with a maximum S_{11} at -6.1 dB, the third notched band at 1.68-1.78 GHz with a maximum S_{11} at -7.3 dB, the fourth notched band at 1.95-2.24 with S_{11} max at -7.5 GHz, the

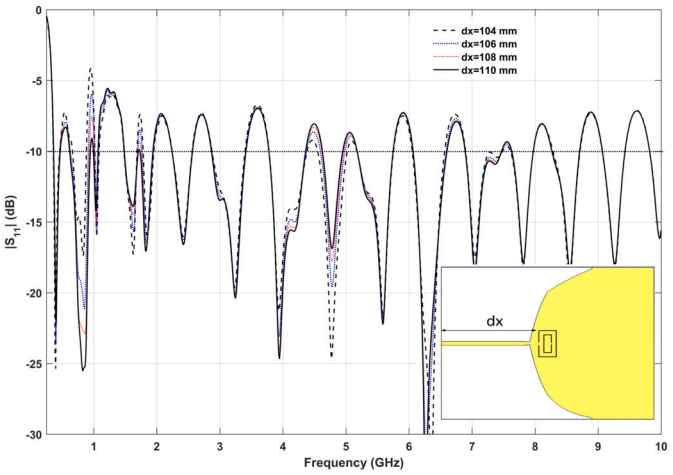

Fig. 5. Reflection coefficient Monopole antenna with variation dx from CSRR.

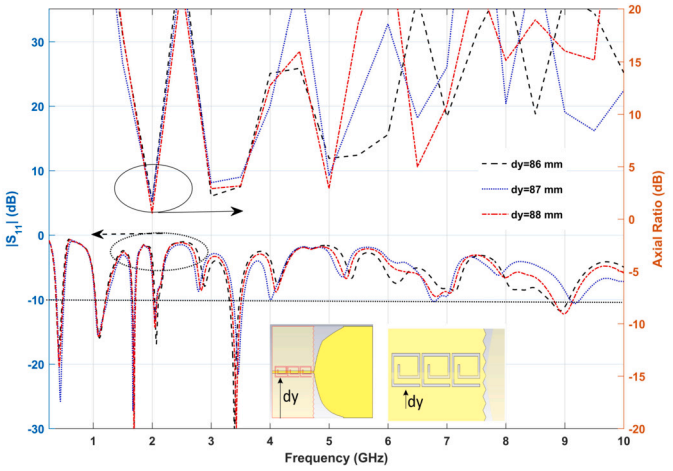

Fig. 6. Simulated S_{11} and axial ratio performance with variations in the dy-position of the rectangular spiral structure.

fifth notched band at 2.56-2.7 GHz with S_{11} max at -7.29, and the sixth notched band at 3.39-3.59 GHz with S_{11} max at -6.72. By modifying the placement and dimensions of the CSRR, it is feasible to generate numerous notched frequency bands at the patch's base, close to the supply end. In addition, the performance of the notched frequency band can be also evaluated by employing a rectangular or circular SRR structure, as well as various types of metamaterial that are positioned above the supply but can be positioned on the opposite side of the patch.

3.4. The impact of rectangular spiral slot to the notched band and axial ratio performance

Fig. 6 shows the performance of the S_{11} antenna as well as the performance of the antenna's axial ratio when it is given a square complementary spiral construction on the ground and positioned on the opposite side of the microstrip feed line. It is possible to construct a large number of notches frequency bands by adjusting the height of the spiral structure (dy). The initial notched band is observed within a broad range of 0.47 – 1.04 GHz, characterized by a rectangular notch and a peak S_{11} of -0.66 dB. The subsequent notched band is identified at 1.21 – 1.66 GHz, exhibiting a maximum S_{11} of -2.43 dB. The third notched band is observed at 1.72 - 2.04 GHz, with the S_{11} peak at -1.41 dB. Subsequently, the notched band manifests over a broad spectrum, necessitating further investigation into the positioning and quantity of spiral structures within the notched band to ensure that it exclusively appears at the intended frequency while still excluding the desired frequency. Additionally, the antenna can adopt circular polarization in a number of different frequency ranges. At the 2 GHz, for a height of dy = 88 mm, the monopole antenna has an Axial Ratio, AR value of 0.56 dB, while for dy = 87 mm and 86 mm it has an AR of 1.67 dB. An AR bandwidth of less than 3 dB is obtained at 128 MHz. To obtain circular polarization performance, this can be done by modifying the location and size of the square spiral structure.

Fig. 7 presents the performance outcomes of the reflection coefficient and axial ratio of the monopole antenna, emphasizing the changes in the position and height of the rectangular spiral structure located on the opposite side of the microstrip feed line within the ground plane. The implementation of rectangular spiral design can lead to the creation of frequency band notches. When y is 21 mm, 20 mm, 19 mm, and 18 mm, S_{11} -10 dB can be observed at the frequencies of 2.69 GHz, 2.81 GHz, 2.93 GHz, and 3.04 GHz. By adjusting the height of the rectangular spiral construction, it is also possible to generate the circular polarization. The axial ratios lower than 3 dB occur at frequencies ranging from 5.965 GHz to 6.585 GHz, which is around 616 MHz with the minimum AR of 1.11 dB. At 7.5 GHz antenna also have AR 0.97 dB from 7.42 GHz to 7.55 GHz. As a result, optimizing is necessary to attain circulation polarization while also expansion of bandwidth. It is possible to investigate integration of metamaterial structures with other forms such that it generates crisp notched frequency bands and circular polarization performance.

3.5. Surface current performance

Fig. 8 shows the difference in surface current of a monopole antenna with a rectangular spiral structure. Fig. 8(a) is a surface current at a frequency of 1.5 GHz and produces a maximum surface current of 39.68 A/m, while Fig. 8(b) is a surface current at a frequency of 2 GHz and produces a maximum surface current of 215.417 A/m. Fig. 8(c) is a surface current at a frequency of 2.5 GHz producing 61.505 A/m while Fig. 8(d) is a surface current at a frequency of 3 GHz and producing 61.505 GHz. It can be seen from Fig. 8(b) that the surface current concentration at the 2 GHz frequency is highest by providing a rectangular spiral structure which can produce circular polarization.

Fig. 9 shows the surface current at (a) $\theta = 0^0$, (b) $\theta = 90^0$, (c) $\theta = 180^0$, and (d) $\theta = 360^0$. At a frequency of 2 GHz, the antenna exhibits an axial ratio of less than 3 dB, indicating circular polarization. The surface current at 0^0 degrees exhibits identical magnitude but opposite direction compared to the data at 180^0. This also pertains to the surface current at angles of 90^0 and 270^0, ensuring it aligns with circular polarization.

3.6. Radiation pattern performance

Fig. 10 is the performance of the monopole antenna radiation pattern with a comparison of the wavy structure type A, C and D as shown (based on Fig. 3). Fig. 10(a) is a comparison of the radiation pattern at the 2 GHz frequency between Wave type C and A and produces a main lobe magnitude for Type C and A of 5.8 dBi and 6.13 dBi and side-lobe level of -2.4 dB and -4.4 dB. Fig. 10(b) shows a comparison of polar radiation patterns at 3 GHz between wave types A and D, with a main-lobe of 4.1 dBi (Type-A) and 5.75 dBi (Type-D). This means the main-lobe has increased by 1.65 dBi. Fig. 10(c) shows a comparison of polar plots radiation patterns at 8 GHz between Wave Types C and A, resulting in a main-lobe of 7.45 dBi (Type-C) and 5.89 dBi (Type-A), indicating a 1.56 dBi improvement in main-lobe. It can be seen that increasing gain performance by providing waveform variations at the top edge of the antenna patch can occur but varies for each frequency. Optimization needs to be done to reduce the side-lobe level value and maximize the directivity formed.

Figs. 11(a) and (b) illustrate the comparison of Co and cross polarization of a monopole antenna with variations in theta and phi at $\theta = 0^0$ and 90^0. The simulation findings at a frequency of 0.5 GHz indicate that

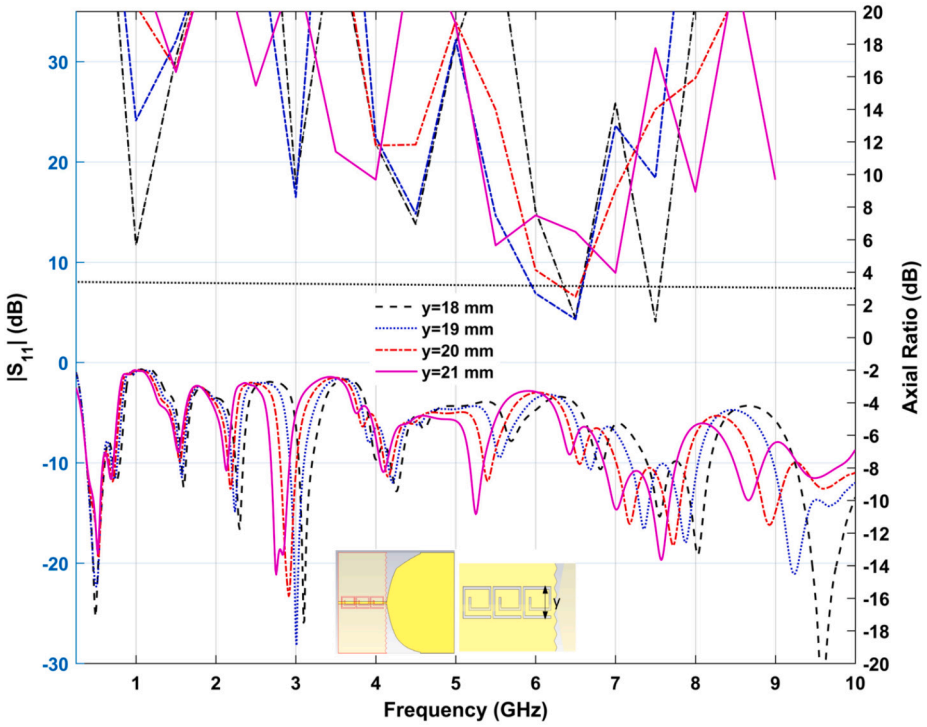

Fig. 7. Effect of the spiral height (y) on the Coefficient reflection and Axial Ratio performance).

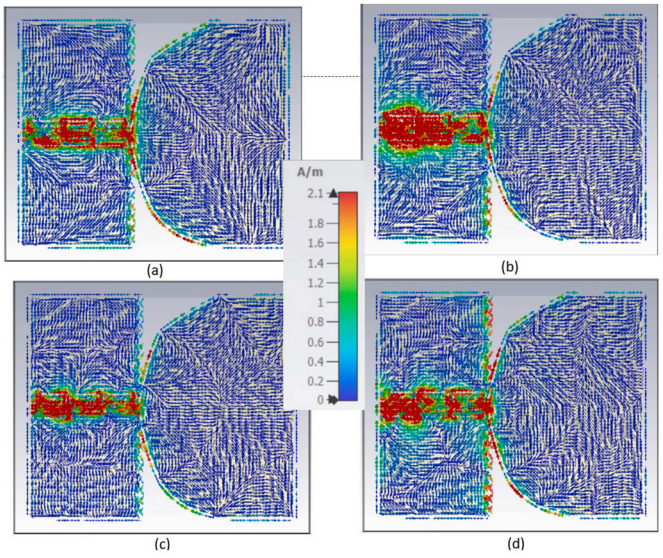

Fig. 8. Surface Current performance at (a) 1.5 GHz, (b). 2 GHz, (c). 2.5 GHz and (d) 3 GHz.

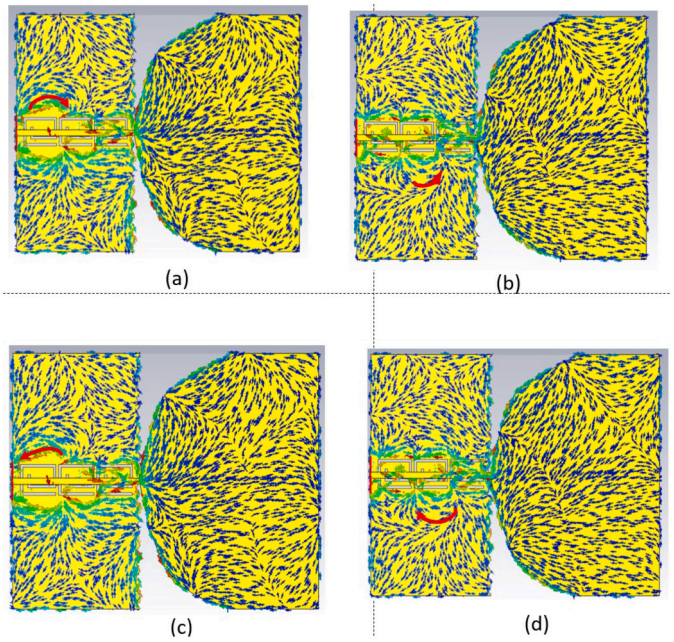

Fig. 9. Surface Current performance at 2 GHz (a) $\theta = 0^0$, (b) $\theta = 90^0$, (c) $\theta = 180^0$, and (d) $\theta = 360^0$.

the mainlobe magnitude of Co-Polarization ($\phi = 0^0$) is 2.52 dB, but the Cross Polarization ($\phi = 90^0$) measures -34.6 dBi. At a frequency of 1 GHz, the main lobe magnitude of Co-Polarization ($\phi = 0^0$) is 3.57 dB, whereas the Cross Polarization ($\phi = 90^0$) is -12.6 dBi. Fig. 11(c) and (d) illustrate the comparison of Co and cross polarization of the monopole antenna with Phi and Theta variations at 0^0 and 90^0. At a frequency of 0.5 GHz, the major lobe magnitude of Co-Polarization ($\theta = 0^0$) is 2.43 dBi, whereas Cross Polarization ($\theta = 90^0$) is -41 dBi. At a frequency of 1 GHz, the mainlobe magnitude of Co-Polarization ($\theta = 0^0$) is 3.38 dBi, whereas Cross Polarization ($\theta = 0^0$) is -28.5 dBi. The results for low frequencies indicate that co- and cross-polarization exhibit substantial variances in their major lobe values.

3.7. Simulated and measured result

Fig. 12 presents a comparison between the data obtained from the simulation and the measurements results taken from the monopole antenna. The findings regarding the performance of the return loss coefficient make it abundantly clear that the results of the measurements closely correspond to the results of the simulations, particularly for frequencies ranging from 0.38 GHz to 12 GHz. Despite this, the results of

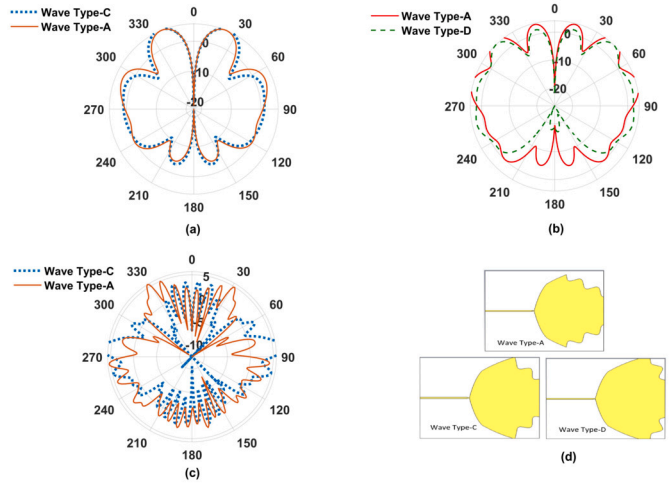

Fig. 10. Radiation Pattern performance in the E-plane at theta 90^0 of Monopole antenna with variation of wave structure on the antenna patch (see Fig. 3).

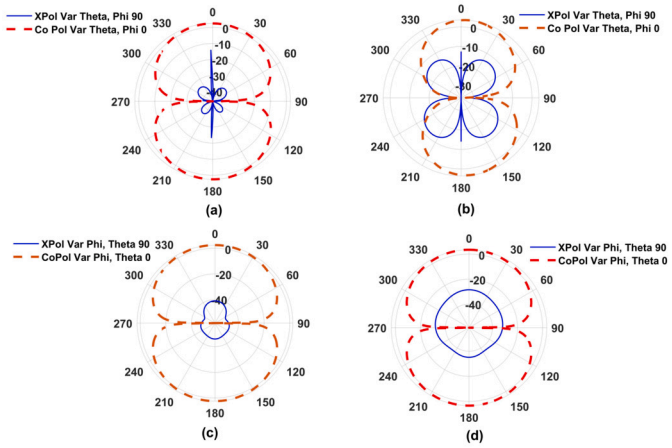

Fig. 11. Co/X-Pol performance of Monopole antenna at frequency (a) 0.5 GHz, (b) 1 GHz, (c) 0.5 GHz and (d) 1 GHz.

the experiments suggest that the antenna has a reflection coefficient that is lower than -10 dB along the frequency range of 0.38 GHz to 20 GHz.

Antennas for through-wall radar applications were also measured, as illustrated in Figs. 13 and 14. The antenna is linked to the VNA SVA 1075X through port 1, and the proximity of metallic objects to the antenna may affect the antenna's reflection coefficient. The antenna's S_{11} can be changed by inserting a difference behind the wall. The antenna is positioned at different x and y coordinates, leading to a range of reflection coefficient values. In Fig. 14, the target's coordinates are indicated by a slightly distinct color image. Thus, monopole antennas can be used to detect objects for through wall radar application.

3.8. The comparison of antennas with related references

Table 2 provides a comparison of antennas that are capable of operating at sub 1 GHz frequencies (low frequency) as well as broad frequencies. On ref [3], [11], [14], the antenna works at sub 1 GHz frequencies. Despite its smaller size, the low-end frequency beneath the antenna exceeds our design specifications and exhibits a narrow bandwidth. The antennas cited in references [15] exhibit a lower low-end frequency compared to the antennas we developed; however, their fractional bandwidth is notably restricted, only 10.36%. Ref [16], [17], [19], [20], [21], [36], [37] dan [38] has a larger size and working in smaller bandwidtht than the antenna we designed. The reference [39], [40], [41], [42], [43], [44], and [45] exhibits a reduced size; however, it

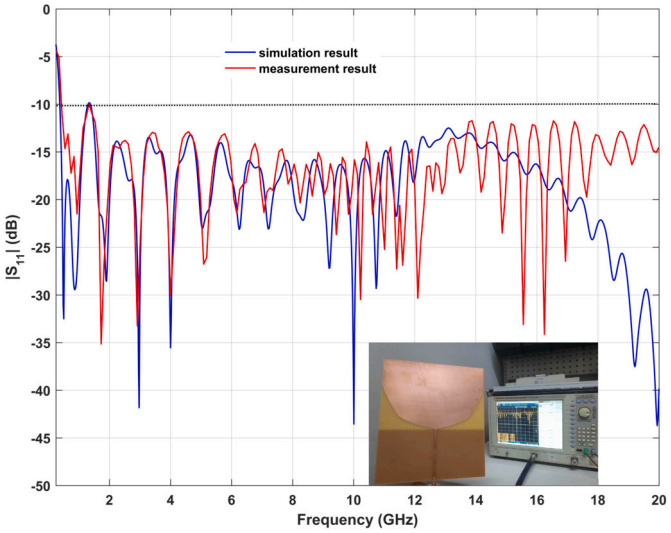

Fig. 12. Simulated and measurement result of monopole antenna.

Fig. 13. Experiment set up for Through Wall Radar application.

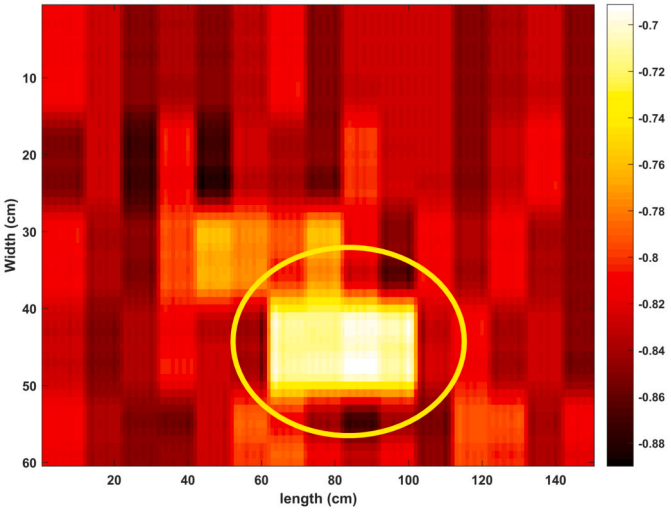

Fig. 14. Detection of radar targets in the xy-planes.

possesses a higher frequency at the lower end and a narrower bandwidth compared to the antenna we developed. Reference [46] features a bigger antenna size compared to our constructed antenna and possesses a fractional bandwidth of merely 22.4%. Reference [47] is smaller in size, with an initial operating frequency of 0.930 GHz and a fractional bandwidth of merely 5.23%. Our antenna has fractional bandwidth 192.5% that work from 0.38 to more than 20 GHz. Antennas with a frequency of less than 1 GHz can be applied for, UHF RFID, GPS L1, hand held termi-

Table 2
Comparison with other relevant References.

Ref	Dim (mm^2)	Substrate	Frequency(GHz)	% Frac-Bandwidth	Gain (dBi)	Application
[3]	162 × 162	Felt	0.902 -0.928 and	4.3	9.3	RFID, ISM, GPS L1
[11]	120 × 120	FR4	0.750 - 1.150 0.563 - 1.587	42.1	3.62	UHF RFID
[14]	120 × 120	FR4	0.620 - 1.410	77	3.7	UHF RFID
[15]	230 × 65	FR4	0.302 - 0.335	10.36	1.76	hand held terminals
[16]	1220 × 1220	polylacticacid	0.040–0.160	120	5	Satellite
[17]	250 × 141	FR4	0.840 - 0.960	13.3	7.3	RFID
[19]	450 × 600	Rogers	0.470-2.80	142.5	7	GPR
[20]	500 × 400	FR4	0.17 - 0.247	36.9	0.98	Boat-Borne GPR
[21]	240 × 240	FR4	0.7 - 2.1	100	2	GPR
[36]	240 × 240	RO4003C	0.918 - 0.926	0.87	9	UHF-UWB
[37]	2880 × 3500	Metal plate	0.20 - 0.220	166.6	13.5	Vehicle
[38]	280 × 250	Teflon	0.220 - 0.950	124.8	2.5	Radio station, GSM
[39]	77 × 35	FR4	1.440 - 18.800	171.5	7	DVB-H, DCS, WIMAX
[40]	150 × 150	FR4	1.710 - 1.880	9.47	5	LTE, DTV
[41]	110 × 160	Roger 4003	0.9 - 2.4	90.9	6	ISM Band
[42]	51 × 82	Teflon	0.42 0.436	3.73	4.3	ISM 433 MHz
[43]	172 × 196	FR4	0.42 - 5.5	171.6	7.96	GPR
[44]	70 × 75	Alumunium	0.473 and 0.420	11.97	1.3	ISM 433 (WSN)
[45]	40 × 50	FR4	0.760 -0.886	15.3	2.2	LTE
[46]	250 × 250	N/A	0.768 - 0.962	22.4	9.8	RFID
[47]	100 × 150	FR4	0.930 - 0.980	5.23	-	Sensor Network
This work	240 × 200	FR4	0.38 - More than 20	192.5	7.45	UHF, TWR, SWB

nal, UHF-UWB, LTE, DTE, ISM 433 MHz, GPR, vehicles, Sensor networks and others so that it can be used for many applications.

4. Conclusion

This study presents a simulation of a monopole antenna designed for SWB frequencies, achieving S11 less than -15 dB throughout nearly the whole frequency range of 0.37 to 20 GHz, resulting in an impedance bandwidth of 192%. Numerous parametric studies of monopole antennas have been performed by altering the wave structure on the upper surface of the patch antenna, the height of the ground plane, the configuration of the CSRR, and the rectangular spiral slot to yield various performances of the reflection coefficient and directivity of the antenna. The shorter microstrip feeding line and ground plane, the worse reflection coefficient performance, although it provides strong gain at low frequencies. By providing a rectangular CSRR structure at the base of the patch and rectangular spiral slots in the ground plane and on the opposite side of the feeder antenna, Notched frequency bands and circular polarization also can be generated. The designed monopole antenna has great potential to be developed for UHF, UWB, RADAR and SWB frequency applications

CRediT authorship contribution statement

Nurhayati Nurhayati: Writing – review & editing, Software, Methodology, Conceptualization. **Fitri Yuli Zulkifli:** Writing – original draft, Data curation. **Ali Hanafiah Rombe:** Software, Methodology, Conceptualization. **Rohim Aminullah Firdaus:** Writing – original draft, Formal analysis. **Muhammad Fauzan Edy Purnomo:** Writing – review & editing. **Minh Thuy Le:** Validation, Formal analysis, Data curation. **Ahmed J.A. Al-Gburi:** Software, Methodology, Conceptualization.

Declaration of competing interest

The authors declare that they have no known competing financial interests or personal relationships that could have appeared to influence the work reported in this paper.

Data availability

The data that has been used is confidential.

References

[1] M. Ayaz, M. Ammad-uddin, I. Baig, M. Aggoune, S. Member, Wireless sensor' s civil applications, prototypes, and future integration possibilities: a review 18 (1) (2018) 4–30.
[2] Jayendra Kumar, Compact MIMO antenna, Microw. Opt. 48 (12) (2006) 2611–2615, https://doi.org/10.1002/mop.
[3] Q. Liu, S. Zhong, Y. Yu, W.S. Zhao, G. Wang, Platform-tolerant nested-slot RFID tag antenna based on jigsaw-shaped metasurface, IEEE Antennas Wirel. Propag. Lett. 21 (5) (2022) 943–947, https://doi.org/10.1109/LAWP.2022.3152621.
[4] A.K. Chaudhary, M. Manohar, A modified SWB hexagonal fractal spatial diversity antenna with high isolation using meander line approach, IEEE Access 10 (2022) 10238–10250, https://doi.org/10.1109/ACCESS.2022.3144850.
[5] X. Zhang, M. Derival, U. Albrecht, Y. Ampatzidis, Evaluation of a ground penetrating radar to map the root architecture of HLB-infected citrus trees, https://doi.org/10.3390/agronomy9070354, 2019, pp. 1–21.
[6] M. Kashanianfard, K. Sarabandi, Vehicular optically transparent UHF antenna for terrestrial communication, IEEE Trans. Antennas Propag. 65 (8) (2017) 3942–3949, https://doi.org/10.1109/TAP.2017.2717973.
[7] H. Lee, J. Tak, J. Choi, Wearable antenna integrated into military berets for indoor/outdoor positioning system, IEEE Antennas Wirel. Propag. Lett. 16 (2017) 1919–1922, https://doi.org/10.1109/LAWP.2017.2688400.
[8] S. Saleh, T. Saeidi, N. Timmons, B. Alali, F. Razzaz, A.A. Althuwayb, High-performance UWB Vivaldi antenna on FR4: a cost-effective solution for wearable technologies, Results Eng. 25 (o) (February 2025) 104230, https://doi.org/10.1016/j.rineng.2025.104230.
[9] T. Saeidi, S.N. Mahmood, S. Saleh, N. Timmons, A.J.A. Al-Gburi, F. Razzaz, Ultra-wideband (UWB) antennas for breast cancer detection with microwave imaging: a review, Results Eng. 25 (o) (February 2025), https://doi.org/10.1016/j.rineng.2025.104167.
[10] V.R. Rentapalli, B. Roy, A low-profile wideband meta-surface based microstrip antenna for 5G wireless communications, Results Eng. 24 (o) (October 2024) 103146, https://doi.org/10.1016/j.rineng.2024.103146.
[11] P. Janpangngern, C. Phongcharoenpanich, Circularly polarized single-fed wide-slot antenna for UHF RFID reader, in: 2017 Int. Symp. Antennas Propagation, ISAP 2017, vol. 2017-Janua, 2017, pp. 1–2.
[12] N.O. Parchin, H.J. Basherlou, R.A. Abd-Alhameed, J.M. Noras, Dual-band monopole antenna for RFID applications, Future Internet 11 (2) (2019), https://doi.org/10.3390/fi11020031.
[13] A. Pal, D. Ahmad, S. Pal, A.N. Ghazali, Efficient and low SAR dual functional wearable antenna in RFID ISM and GPS L1 bands for positioning applications, Wirel. Netw. 30 (6) (2023) 5187–5199, https://doi.org/10.1007/s11276-023-03238-3.
[14] N. Supreeyatitikul, N. Teerasuttakorn, P. Boontamchauy, M. Rattanasuttikan, A compact printed wideband circularly polarized slot antenna for universal UHF RFID reader, in: 14th Eur. Conf. Antennas Propagation, EuCAP 2020, 2020, pp. 4–8.
[15] D. Wang, et al., A high-efficiency broadband omnidirectional UHF patch antenna applying surface plasmon polaritons for handheld terminals, IEEE Antennas Wirel. Propag. Lett. 17 (2) (2018) 283–286, https://doi.org/10.1109/LAWP.2017.2786779.
[16] A.D. Johnson, J.A. Caripidis, S.B. Venkatakrishnan, M. Ali, J.L. Volakis, Deployable inverted-hat monopole with 3:1 constant gain bandwidth, IEEE Antennas

Wirel. Propag. Lett. 19 (6) (2020) 935–938, https://doi.org/10.1109/LAWP.2020.2983746.
[17] Y. Pan, L. Zheng, H.J. Liu, J.Y. Wang, R.L. Li, Directly-fed single-layer wideband RFID reader antenna, Electron. Lett. 48 (11) (2012) 607–608, https://doi.org/10.1049/el.2012.1140.
[18] X. Liu, Y. Liu, M.M. Tentzeris, A novel circularly polarized antenna with coin-shaped patches and a ring-shaped strip for worldwide UHF RFID applications, IEEE Antennas Wirel. Propag. Lett. 14 (c) (2015) 707–710, https://doi.org/10.1109/LAWP.2014.2378513.
[19] H.S. Senapati, P. Chongder, S. Maiti, Design and simulation of a parasitic patch loaded novel broadband antipodal Vivaldi antenna for GPR applications, in: 2022 IEEE Microwaves, Antennas, Propag. Conf., MAPCON 2022, 2022, pp. 886–890.
[20] J. Tong, Y. Guo, C. Ji, X. Chai, Q. Zhao, A compact wideband semi-elliptical dipole antenna for boat-borne GPR, IEEE Trans. Antennas Propag. 70 (12) (2022) 11496–11504, https://doi.org/10.1109/TAP.2022.3209666.
[21] H. Cheng, H. Yang, Y. Li, Y. Chen, A compact Vivaldi antenna with artificial material lens and sidelobe suppressor for GPR applications, IEEE Access 8 (2020) 64056–64063, https://doi.org/10.1109/ACCESS.2020.2984010.
[22] B. Roy, S.K. Chowdhury, A.K. Bhattacharjee, Symmetrical hexagonal monopole antenna with bandwidth enhancement under UWB operations, Wirel. Pers. Commun. 108 (2) (2019) 853–863, https://doi.org/10.1007/s11277-019-06433-8.
[23] N. Nurhayati, F.Y. Zulkifli, E. Setijadi, B.E. Sukoco, M.N.M. Yasin, A.M. De Oliveira, Bandwidth, gain improvement, and notched-band frequency of SWB wave coplanar Vivaldi antenna using CSRR, IEEE Access 12 (o) (February 2024) 16926–16938, https://doi.org/10.1109/ACCESS.2024.3359168.
[24] S.A. Adamu, T. Masri, W.A.W.Z. Abidin, K.H. Ping, Band-notched antipodal Vivaldi antenna using edge-located vias mushroom EBG structure for ultra wideband applications, Int. J. Innov. Technol. Explor. Eng. 9 (4) (2020) 2455–2459, https://doi.org/10.35940/ijitee.c8572.029420.
[25] A.S. Abbas, M.K. Abdelazeez, A dual band notch planar SWB antenna with two vertical sleeves on slotted ground plane, in: 2016 IEEE Antennas Propag. Soc. Int. Symp. APSURSI 2016 - Proc., no. 2, 2016, pp. 2131–2132.
[26] L. Zhao, et al., Compact circular-shaped MIMO antenna covers UWB bandwidth with four frequently-used band-notched characteristics for multi-scenario applications, IEEE Access 12 (o) (February 2024) 32762–32771, https://doi.org/10.1109/ACCESS.2024.3371571.
[27] A. Valizade, C. Ghobadi, J. Nourinia, M. Ojaroudi, A novel design of reconfigurable slot antenna with switchable band notch and multiresonance functions for uwb applications, IEEE Antennas Wirel. Propag. Lett. 11 (2012) 1166–1169, https://doi.org/10.1109/LAWP.2012.2218271.
[28] Z. Zhao, et al., A miniaturized wearable antenna with five band-notched characteristics for medical applications, IEEE Antennas Wirel. Propag. Lett. 22 (6) (2023) 1246–1250, https://doi.org/10.1109/LAWP.2023.3237714.
[29] S.K. Bairappaka, A. Ghosh, J. Kumar, A. Bhattacharya, A compact triple band circular polarized slotted microstrip patch antenna with low frequency ratio, Int. J. RF Microw. Comput. Eng. 32 (12) (2022) 23410, https://doi.org/10.1002/mmce.23410.
[30] X. Cheng, Y. Yao, J. Yu, X. Chen, Circularly polarized substrate-integrated waveguide tapered slot antenna for millimeter-wave applications, IEEE Antennas Wirel. Propag. Lett. 16 (61474112) (2017) 2358–2361, https://doi.org/10.1109/LAWP.2017.2718240.
[31] Y.F. Cao, S.W. Cheung, T.I. Yuk, Dual-cap mushroom-like metasurface used in CP reconfigurable monopole antenna for performance enhancement, IEEE Trans. Antennas Propag. 63 (12) (2015) 5949–5955, https://doi.org/10.1109/TAP.2015.2489682.
[32] M. Mantash, M.B. Kakhki, T.A. Denidni, Millimeter-wave circularly polarized Vivaldi antenna using simple single layer 2D FSS polarizer 3 (2018) 31–32.
[33] L. Zhang, S. Gao, Q. Luo, P.R. Young, Q. Li, Wideband loop antenna with electronically switchable circular polarization, IEEE Antennas Wirel. Propag. Lett. 16 (c) (2017) 242–245, https://doi.org/10.1109/LAWP.2016.2570859.
[34] F.Y. Zulkifli, A.I. Wahdiyat, A. Zufar, N. Nurhayati, E. Setijadi, Super-wideband monopole printed antenna with half-elliptical-shaped patch, Telecom 5 (3) (2024) 760–773, https://doi.org/10.3390/telecom5030038.
[35] G.S. Reddy, A. Kamma, S.K. Mishra, J. Mukherjee, Compact bluetooth/UWB dual-band planar antenna with quadruple band-notch characteristics, IEEE Antennas Wirel. Propag. Lett. 13 (2014) 872–875, https://doi.org/10.1109/LAWP.2014.2320892.
[36] J. Zhang, Z. Shen, Dual-band shared-aperture UHF/UWB RFID reader antenna of circular polarization, IEEE Trans. Antennas Propag. 66 (8) (2018) 3886–3893, https://doi.org/10.1109/TAP.2018.2839883.
[37] H. Shen, J. Yang, X. Shen, P. Peng, S. Li, X. Yin, A compact broadband monopole tapered slot antenna with high field uniformity for vehicle EMC test from 20 to 220 MHz, IEEE Antennas Wirel. Propag. Lett. 22 (8) (2023) 1783–1787, https://doi.org/10.1109/LAWP.2023.3264460.
[38] D. Qin, B. Sun, R. Zhang, VHF/UHF ultrawideband slim monopole antenna with parasitic loadings, IEEE Antennas Wirel. Propag. Lett. 21 (10) (2022) 2050–2054, https://doi.org/10.1109/LAWP.2022.3190015.
[39] K.R. Chen, C.Y.D. Sim, J.S. Row, A compact monopole antenna for super wideband applications, IEEE Antennas Wirel. Propag. Lett. 10 (2011) 488–491, https://doi.org/10.1109/LAWP.2011.2157071.
[40] A.N. Kulkarni, S.K. Sharma, Frequency reconfigurable microstrip loop antenna covering LTE bands with MIMO implementation and wideband microstrip slot antenna all for portable wireless DTV media player, IEEE Trans. Antennas Propag. 61 (2) (2013) 964–968, https://doi.org/10.1109/TAP.2012.2223433.
[41] L.A. Berge, M.T. Reich, B.D. Braaten, A compact dual-band bow-tie slot antenna for 900-MHz and 2400-MHz ISM bands, IEEE Antennas Wirel. Propag. Lett. 10 (2011) 1385–1388, https://doi.org/10.1109/LAWP.2011.2177954.
[42] W. Liu, Z. Zhang, Z. Feng, ISM 433-MHz miniaturized antenna using the shielding box of mobile terminals, IEEE Antennas Wirel. Propag. Lett. 11 (2012) 330–333, https://doi.org/10.1109/LAWP.2012.2191379.
[43] K.K. Ajith, A. Bhattacharya, A novel compact superwideband bowtie antenna for 420 MHz to 5.5 GHz operation, IEEE Trans. Antennas Propag. 66 (8) (2018) 3830–3836, https://doi.org/10.1109/TAP.2018.2836382.
[44] X. Wu, Z. Zheng, A novel compact microstrip antenna embedded with magneto-dielectric ferrite materials for 433 MHz band applications, in: 13th Eur. Conf. Antennas Propagation, EuCAP 2019, no. EuCAP, 2019, pp. 13–16.
[45] M.S. Sharawi, S.S. Iqbal, Y.S. Faouri, An 800 MHz 2× 1 compact MIMO antenna system for LTE handsets, IEEE Trans. Antennas Propag. 59 (8) (2011) 3128–3131, https://doi.org/10.1109/TAP.2011.2158958.
[46] M. Manohar, R.S. Kshetrimayum, A.K. Gogoi, Printed monopole antenna with tapered feed line, feed region and patch for super wideband applications, IET Microw. Antennas Propag. 8 (1) (2014) 39–45, https://doi.org/10.1049/iet-map.2013.0094.
[47] M. Hasegawa, S. Sodenaga, H. Shimasaki, An annular patch circularly polarized antenna in 920-MHz band, in: 2020 Int. Symp. Antennas Propagation, ISAP 2020, 2021, pp. 563–564.